Nanoscale

Accepted Manuscript

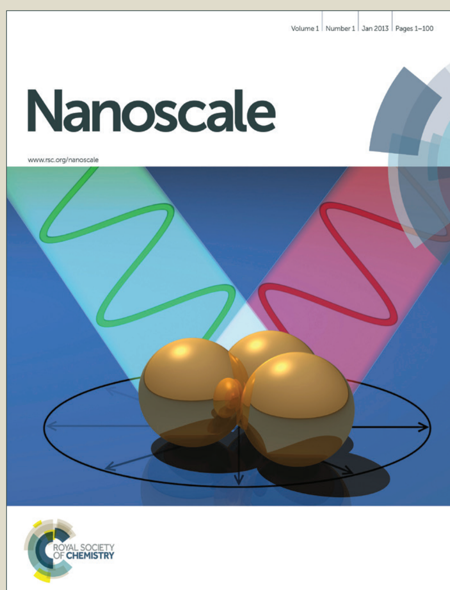

This is an *Accepted Manuscript*, which has been through the Royal Society of Chemistry peer review process and has been accepted for publication.

Accepted Manuscripts are published online shortly after acceptance, before technical editing, formatting and proof reading. Using this free service, authors can make their results available to the community, in citable form, before we publish the edited article. We will replace this *Accepted Manuscript* with the edited and formatted *Advance Article* as soon as it is available.

You can find more information about *Accepted Manuscripts* in the Information for Authors.

Please note that technical editing may introduce minor changes to the text and/or graphics, which may alter content. The journal's standard Terms & Conditions and the Ethical guidelines still apply. In no event shall the Royal Society of Chemistry be held responsible for any errors or omissions in this *Accepted Manuscript* or any consequences arising from the use of any information it contains.

ROYAL SOCIETY OF CHEMISTRY

www.rsc.org/nanoscale

Please do not adjust margins

Nanoscale

ARTICLE

Towards defect-free 1-D GaAs/AlGaAs Heterostructures based on GaAs nanomembranes

Received 00th January 20xx,
Accepted 00th January 20xx

DOI: 10.1039/x0xx00000x

www.rsc.org/

G. Tutuncuoglu,[a] M. de la Mata[b,c], D. Deiana[d], H. Potts[a] , F. Matteini[a], J. Arbiol[b,e] and A. Fontcuberta i Morral[a]

We demonstrate the growth of defect-free zinc-blende GaAs nanomembranes by molecular beam epitaxy. Our growth studies indicate a strong impact of As_4 re-emission and shadowing in the growth rate of the structures. The highest aspect ratio structures are obtained for pitches around 0.7-1 µm and a gallium rate of 1 Å/s. The functionality of the membranes is further illustrated by the growth of quantum heterostructures (such as quantum wells) and the characterization of their optical properties at the nanoscale. This proves the potential of nanoscale membranes for optoelectronic applications.

Introduction

Nanostructures have expanded the functionality of semiconductors in a large variety of areas, ranging from fundamental science to sensing and energy harvesting.[1–6] This increased functionality is generally provided by the small dimensions. For example, the small diameter of nanowires enables an effective strain relaxation, allowing defect-free epitaxy of lattice mismatched materials and the fabrication of new designs of heterostructures.[7–10] In addition to the size, the shape of nanostructures such as nanowire, nanotree[11], tripod[12,13],tetrapod[14,15] or membrane[16–18] provides an opportunity to engineer the functionality. As an example, depending on the diameter, nanowires can host leaky modes or Fabry-Perot resonances, resulting in an enhancement of light absorption and facilitating lasing[18] GaN based nanosheets/nanowalls have proven to be promising candidates for light emitting diode (LED) applications.[19,20] On the same line, it has been shown that nanoscale membranes can enhance second-harmonic generation combining a geometric with a nanoscale size effect.[21]

Polytypism corresponds to the existence of different crystal phases in a material with the same composition. It is an inherent phenomenon in the growth of nanostructures, including nanoparticles, nanowires and nanoscale membranes. The control of polytypism, named crystal-phase engineering, has emerged as a way to capitalize the ability of changing the crystal phase in order to modify the functional properties. Several strategies have been used for the synthesis of single phase nanowires including: careful adjustment of the growth conditions,[22–25] introduction of an additional element to the growth system[26], doping[27] or modifying the growth catalyst by changing the growth conditions.[28] Even though crystal-phase engineering has made extreme progresses in the last 10 years, not all materials systems or growth methods can be controlled completely. In particular, the control of the tiniest defects in III-V semiconductor nanostructures such as twin defects and stacking faults is still challenging. Several works show that twins and stacking faults are detrimental for electronic and optical properties,[29,30] urging for a proper control of the structure to the twin/stacking-fault limit.[22,31,32]

Twin formation in zinc-blende GaAs nanowires has been carefully investigated in the case of selective area epitaxy (SAE). [33–35] SAE of GaAs nanowires starts with a truncated tetrahedral shape forming inclined (1 1 0) facets with respect to (1 1 1)B. The initial nanoscale tetrahedra exhibit their long axis in either <11-2> or <2-1-1> directions. Only the former group of tetrahedra are found to be defect-free.[33,34] However, the development of the <11-2> oriented tetrahedron into a nanowire with hexagonal cross-section and vertical facets inherently results in the loss of defect-free structures. To the best of our knowledge, defect-free SAE GaAs nanowires have not been produced so far. Recently, Chi *et al* used the directionality of twin-free growth to obtain defect-free SAE GaAs nanosheets/nanomembranes by orienting them in the <11-2> direction by metal organic chemical vapour deposition (MOCVD) and investigated their electronic and optical properties. [36,37,38] Here, we optimize the SAE conditions in molecular beam epitaxy, MBE, to obtain high aspect ratio nanoscale membranes. Defect-free

[a.] *Laboratory of Semiconductor Materials, Ecole Polytechnique Fédérale de Lausanne, EPFL, 1015 Lausanne, Switzerland*
[b.] *Institut Català de Nanociència i Nanotecnologia (ICN2), Campus UAB, 08193 Bellaterra, Catalonia, Spain*
[c.] *Institut de Ciència de Materials de Barcelona, ICMAB-CSIC, Campus de la UAB, 08193 Bellaterra, Catalonia, Spain*
[d.] *Centre Interdisciplinaire de Microscopie Electronique, Ecole Polytechnique Fédérale de Lausanne, EPFL, 1015 Lausanne, Switzerland*
[e.] *Institució Catalana de Recerca i Estudis Avançats (ICREA), 08010 Barcelona, Catalonia, Spain*
† Footnotes relating to the title and/or authors should appear here.
Electronic Supplementary Information (ESI) available: [details of any supplementary information available should be included here]. See DOI: 10.1039/x0xx00000x

Nanoscale Accepted Manuscript

Please do not adjust margins

structures are obtained when the long axis is oriented both in the <11-2> and <2-1-1> directions, as demonstrated by transmission electron microscopy. We extend the functionality of these nanostructures by creating quantum heterostructures, which we characterize by photo (PL) and cathodoluminescence (CL).

Experimental Details

GaAs nanoscale membranes were grown using a solid source MBE system, DCA P600. The substrates were undoped (111)B GaAs wafers covered with a 30 nm SiO_2 mask deposited by plasma enhanced chemical vapour deposition, PECVD. The patterns on the wafers were defined by e-beam lithography on an e-beam resist 50% ZEP and transferred by dry etching with a mixture of CH_3/SF_6 gases. The patterns consist of stripe openings with 100 nm width and 5 µm length, oriented in <11-2> and <2-1-1> directions with varying pitches. Six pattern groups were fabricated on a 2 inch wafer. Prior to the loading to MBE machine, the substrates were cleaned by exposing them to an O_2 plasma, and sonicating them in Acetone and Iso-Propyl Alcohol. Upon loading in the MBE system and before transferring to the growth chamber, they were degassed for 2 hours at 400 °C of manipulator temperature in ultra-high vacuum conditions. In the growth chamber, they were heated up to 640 °C for 30 min under an As_4 flux in order to ensure that the openings are free of native oxide.

During the growth, a rotation speed of 7 RPM was applied. The substrate temperature was measured with a pyrometer. Growth was performed in a range of nominal Ga rates 0.3 A/s - 1 Å/s, as measured on (100) GaAs substrates at 600 °C by Reflection high-energy electron diffraction, RHEED. Samples were cooled under As_4 flow and transferred out from the growth chamber at 200 °C.

The morphology and dimensions of the grown samples were analysed with Atomic Force Microscopy (AFM) and Scanning Electron Microscopy (SEM). Images are analysed using Nanoscope Analysis software for AFM, and image processing package ImageJ[39] for SEM. In order to analyse the crystal structure of the nanomembranes two orthogonal lamellas were prepared by focus ion beam (FIB), i.e., the [1-10] and [112], allowing the study of the projected length and width of the membranes along the mentioned directions. The crystal structure of the membranes was analysed by atomic resolution high angle annular dark field (HAADF) scanning transmission electron microscopy (STEM) on the above FIB cuts by using a Titan 300KeV low base (LMA-INA) probe corrected microscope and a double corrected Titan Themis (CIME). For these we characterized a front view along the [1-10] zone axis, and by tilting 19° the [112] FIB cut we were able to analyse the [111] lateral projection where the quantum well structures appeared perpendicular to the visual plane. To completely understand the morphology and distribution of the AlGaAs shell, a 3D atomic model created by the Rhodius package is provided.[40,41] The optical properties of the membranes and quantum heterostructures were characterized by low-temperature photoluminescence, PL, in a closed loop cryostat with a base temperature of 3.85K (Attocube 700) and by low temperature spectrally resolved cathodoluminescence, CL (Attolight Rosa).

Results and Discussion

We studied the growth of GaAs on nanoscale longitudinal openings under SAE conditions and optimized them in order to obtain high aspect-ratio structures. Selectivity of epitaxy on GaAs with respect to the oxide mask is obtained when the sticking coefficient of gallium adatoms on SiO_2 is so low that adsorbed gallium is desorbed from the surface or the diffusion length is high enough so that the gallium adatoms will diffuse to the GaAs openings where they contribute to the epitaxy. The sticking coefficient and diffusion length are controlled through the temperature of the substrate and the incoming atomic fluxes. Diffusion length of gallium adatoms increases with temperature, while the sticking coefficient of gallium on SiO_2 is inversely proportional to it. The diffusion length of gallium adatoms diminishes when the gallium rate or arsenic flux is increased.[42] As the substrate temperature is the main parameter determining selectivity between GaAs and SiO_2, we started by finding the optimal substrate temperature range for SAE.

Temperature Dependency

In order to optimize the growth temperature and decrease the amount of parasitic growth, a sample series with varying temperatures have been grown under 0.3 A/s growth rate and V/III ratio of 60. A temperature between 625 and 635 °C was found to be ideal. For temperatures below 625°C there was significant parasitic growth dominating the region outside the pattern and the structures were not uniform. For temperatures above 635°C, it was not possible to obtain high aspect-ratio structures due to the increasing decomposition rate of GaAs. In addition, we could observe twining defects at the side facets and decomposition induced defects on the dielectric layer. (See SI)

V/III Dependency

We turn now to the dependency of the morphology of the nanoscale membranes on V/III ratio. We start by varying the arsenic flux under a low gallium rate and follow by varying the gallium rate. The gallium rate was fixed initially to 0.3 Å/s, which was reported to be the ideal growth rate for SAE.[42] The arsenic flux was varied between 7.3x10^{-6} and 1 x 10^{-6} Torr, with the expectation to obtain higher axial rates for a higher arsenic flux. We could not observe any trend on the morphology or the axial growth rates within the covered the range (See SI). Moreover, all structures grown under a gallium rate of 0.3 Å/s did not exhibit vertical {110} sidewalls, their height was around 100 nm and increasing the growth time did not facilitate the axial growth (see SI). A change in the arsenic flux did not make any significant effect on the faceting of the structures. In contrast to the work of Chi *et al* by MOCVD, vertical {110} sidewalls were not achieved at low V/III ratio by lowering arsine flow.[36]

Next, we reduced the V/III ratio by increasing the gallium rate while keeping the As_4 flux constant. A SEM image of a typical membrane array obtained under 1Å/s gallium rate, along with the

Nanoscale Accepted Manuscript

This journal is © The Royal Society of Chemistry 20xx

Please do not adjust margins

corresponding 3D model of the morphology and faceting are shown in Fig. 1. The lateral flat facets correspond to planes of the {110} family, respectively (1-10) and (-110). There are two inclined top facets. The shorter facet is inclined 55° with respect to the substrate surface. It presents a flat surface corresponding to a (-2-2-1) plane. The longest facet is inclined 19.5° with respect to the substrate. In this case, it is formed by two {110} planes corresponding to (0-11) and (-101) surfaces. Furthermore, the width of the membranes is larger than the original 100 nm opening in the mask. This indicates a non-negligible radial growth which is also observed in the cross-section TEM analysis, shown later. The average height of the structures in Fig. 1a is 900 nm. For the given growth duration, nominal planar growth thickness is 250 nm. This means there is an increase of a factor 3.6 in the axial growth rate.

The dependence of the faceting and dimensions of the nanoscale membranes on the gallium flux is illustrated in Fig. 2a. All SEM images correspond to 1h growth. Vertical {110} sidewalls are achieved only for higher gallium rates, starting at 0.5 Å/s. The height and aspect ratio of the membranes increases with the gallium rate. This indicates that membrane growth occurs under gallium-limited conditions as for typical planar epitaxy and opposite to catalyst-free nanowire growth.[43]

Pitch Dependency

In order to obtain further insights in the growth mechanisms, we looked at the growth rate of the membranes as a function of the pitch, for different gallium rates, shown in Fig. 2b. As discussed here below, the gallium rate does not only change the faceting but also the growth dynamics. We observe different pitch dependencies for different gallium fluxes. As shown in Fig. 2b top, the height of the membranes decreases for larger pitches for a gallium rate of 0.3 Å/s. A different trend is observed for higher gallium rates. As we increase the gallium rate, this decreasing trend evolves into two distinctive regimes. Fig. 2b down shows the example of gallium rate of 0.7 Å/s. The growth rate of the membranes increases as a function of the pitch for pitch values between 200 and 700 nm and saturates till a pitch of 1000 nm. This pitch dependence resembles what has been previously observed for InAs, GaP and GaAs nanowire arrays.[44–47] The increase of the growth rate with the pitch would be consistent with the competitive regime: the distance between the membranes is smaller than the range from which the adatoms contributing to growth are collected. For pitches larger than 1000 nm, the growth rate decreases steadily with the pitch. This seems to be inconsistent with the competitive regime picture. In order to understand this trend in greater detail we need to consider the different pathways of gallium adatoms and As_4 that can contribute to growth: direct flux impingement on the membranes, re-adsorption from the substrate, re-adsorption from the neighbouring membranes, surface diffusion through the mask and surface diffusion through the sidewalls.

We start by discussing the trend observed at longer pitches for the Ga rate 0.7 Å/s. The decrease in the membrane height for an increasing pitch reveals the loss of adatoms contributing to growth. These can only be re-adsorption of atoms re-emitted from the neighbouring membranes. It has been shown that this is mainly As_x (x=2 or 4) and not Ga.[48] We therefore conclude that re-emission of As_x adatoms is a non-negligible contribution to the growth of the membranes.

We turn now to the analysis of the trend observed for pitches shorter than P=700 nm for the Ga rate of 0.7 Å/s. Here, there is a loss of atoms contribution when the pitch is reduced. There could be two origins: (i) shadowing between the membranes which would reduce the incoming flux on and around the membrane and (ii) the distance between membranes is smaller than the Ga adatom diffusion length. It has been shown that the diffusion length of gallium on SiO_2 is around 200 nm at 630°C, shorter than half of the shortest pitch, P=500 nm. This means that the collection area of the membranes will not overlap with each other. We consider now the effect of shadowing. Since the incoming flux arrives at an angle of 45°, each membrane shadows a distance which is equal to its height, H. This means that for the condition of $P/2 < H \leq P$ shading will be pronounced. For the lowest values of pitch where we see an increasing trend, P is smaller than 700 nm. There is significant shadowing which decreases as the distance between membranes increases. Shadowing will reduce the direct flux impingement on top or side facets depending on the distance. When P = H each membrane completely masks the region with its neighbour. After 700 nm we observe a decreasing trend again because shadowing is no longer pronounced and re-adsorption from the neighbouring side facets diminish as the distance between the membranes would increase.

Finally, we discuss the contribution to the growth via surface diffusion from the sidewalls. This should not depend on the distance between the membranes, but only on the length and type of facets. It has been shown that the diffusion length of gallium on GaAs is the lowest on (113)B surfaces, followed by (001), (111)B and (111)A. It is the longest for (110) surfaces.[42,49,50] This means that when facets of the {110} are formed, diffusion of gallium adatoms along these facets should not limit the membrane growth rate.

GaAs/AlGaAs Heterostructures

In order to demonstrate the functionality of the nanoscale membranes, we used them as templates for more advanced heterostructures. As a first step, we have grown a passivation AlGaAs shell around GaAs core, with a nominal Al concentration of 30%. The AlGaAs shell was further covered by a 3 nm GaAs layer to avoid oxidation. For the growth of the passivation layer, we adjusted the growth conditions.[8] The substrate temperature was decreased to 550 °C and As flux was increased to 7×10^{-6} torr. Following that, we have grown a series of quantum well samples consisting of AlGaAs/GaAs/AlGaAs layers. In Fig. 3, TEM cross-sectional analysis of a GaAs membrane covered by the AlGaAs/GaAs shell and QW structure are shown. These cross-sections correspond to the pattern with 500 nm pitch. In Fig. 3a the longitudinal cross-section in a low-magnification micrograph is shown. The HAADF STEM atomic resolution analysis indicates that the membranes are

Nanoscale Accepted Manuscript

Please do not adjust margins

pure zinc-blende with the vertical growth direction being [-1-11], As polar (an atomic resolution image of the crystal structure is shown at the inset). One small area close to the (-2-2-1) facets shows few twin defects. We attribute the origin of these defects to the existence of imperfections of the pattern especially at the tips of the openings, which cause the formation of heterogeneous nucleation sites and uneven lateral growth, which are also visible at SEM images.

In Fig. 3b, the left part depicts HAADF-STEM general view of the membrane cross-section and on the right, we show a close up of the opening in the mask and demonstrate the perfect epitaxial relation between the GaAs substrate and the membrane. It can be seen that the bottom part of the membrane is slightly thinner compared to the top part and there is radial growth shown by the expansion of the membrane to out of the pattern opening. Since the pitch is defined as the distance from the start of one membrane to its neighbour, the distance between two membranes opposite side facets would be 400 nm. By taking into account the radial growth, the real distance should be around 300 nm. As a consequence, part of the membrane should be exposed to shadowing effects, which should lead to thinner AlGaAs shells at the bottom of the membranes. In Fig. 3c, HAADF-STEM image of the membrane cross-section obtained at 19° is shown. GaAs QWs formed at top and side facets are clearly demonstrated.

In Fig. 3d we show an indexed 3D atomic model of an entire nanomembrane and the corresponding model for the FIB cut in lateral and front views. In Fig. 3e EDX elemental maps of Al and Ga obtained on the nanomembrane cross-section shown in 3c are shown. In Fig S4 (Supp. Info.) EELS elemental maps of Al, Ga and As obtained on the nanomembrane cross-section shown in 3b are shown. It can be clearly seen that an AlGaAs shell is grown conformal around the membrane. We observe a slight gradient of the thickness from the bottom of the structure towards the top. We attribute this to the low diffusion lengths of aluminium and gallium at 550 °C, amplifying the aforementioned shadowing effect. It is also very interesting that we observe the segregation of aluminium at the apex of the top (-101) and (0-11) facets (see SI) which is a commonly observed phenomena at the radial growth of III- V nanowires.[8,51]

PL studies of capped GaAs membranes

The AlGaAs shell has been primarily used to passivate the GaAs core membrane to reduce surface recombination and thereby increase PL intensity. In Fig. 4, the PL spectrum of such a core/shell heterostructure is shown. An SEM image of the measured structure is presented in the inset. The PL measurements are performed at 4K. The free exciton peak of GaAs can be clearly observed at 1.519 eV with a linewidth of 6 meV, indicating the high quality of the GaAs growth and its pure zinc-blende nature. The smaller peak at a lower energy, 1.4861 eV, is attributed to the donor acceptor transitions caused by carbon impurities on GaAs wafer, which is typically observed in commercial GaAs substrates.[42,52] The intensity of this lower energy peak increases when the laser spot is moved out of the pattern.

CL studies of GaAs/AlGaAs heterostructures with Quantum Wells

Following the PL measurements on the GaAs membranes, we continued our studies on quantum wells (QWs) grown on the GaAs membranes, which we analysed by CL. CL consists of the excitation of luminescence by an electron beam in a scanning electron microscopy configuration. The electron beam size is around 5 nm in diameter, enabling high precision excitation maps. The geometry of the membranes, the direction of the incoming flux and the evident diffusion between the facets make it difficult to anticipate the thickness of the QWs at the specific facets. Still, one would expect QWs of different thickness on the top and inclined side facets. In Fig. 5, CL mapping and spectra of a membrane array with heterostructures of the AlGaAs/GaAs/AlGaAs (20nm/8nm/20nm - nominal) layers are shown. In the CL mapping, each colour is assigned to a different detected energy. In the inset, a secondary electron SEM image of the membrane array is presented. As expected, we observe emission at different energies depending on the excited facet. Red corresponds to the emission at 780 nm (1.587 eV), green indicates the emission at 809 nm (1.533 eV) and blue for 813.7 nm (1.524 eV). In Fig. 5b, we plot the four spectra collected in the points assigned with each of the colours in the map. In the map, the truncated facets of the membranes in 19° with respect to the substrate appear in blue. A reduction of the QW thickness according to the angle between the facet normal vector with respect to the nominal value is expected. The emission color-coded in green is more dominant at the (-2-2-1) facets of the nanoscale membranes. These are inclined 55° with respect to the growth substrate so they will receive less amount of flux compared to the other truncated facets which are at 19° with the substrate. Consequently, QW grown on (-2-2-1) facets should be thinner and therefore emit at higher energy. The spectrum colour coded in grey is taken from a region between the membranes in order to check the contribution of the substrate to CL signal. Although the spectrum looks flat when plotted with the same scale of the membrane spectra, it exhibits a very small peak at 828 nm with an intensity 200 times lower, compared to the emission coming from the membrane. As a consequence, in this case we do not have an important contribution from the substrate. We should also comment on the emission linewidth. Micro-photoluminescence measurements on the membranes show that the linewidth of QW emissions is much smaller than on equivalent heterostructures in nanowires (see SI).[8] This is a further signature of the high quality of these heterostructures.

Finally, we would like to comment on the emission plotted in red, which is localized at the membrane tips. Its emission energy is higher than any level of the quantum wells mentioned before. It is also in the range of quantum dots which we previously observed in core/shell GaAs/AlGaAs nanowires.[9] Although in this particular mapping we observe this emission at the corner of the membrane, we have observed it in other locations of the membranes as well as in other samples, i.e. the tips. More thorough studies are needed to

Nanoscale Accepted Manuscript

This journal is © The Royal Society of Chemistry 20xx

understand the origin of these emissions and compare them to those observed in nanowire AlGaAs shells.

Conclusions

In conclusion we have demonstrated the ideal conditions for the growth of defect-free zinc-blende GaAs nanoscale membranes by MBE. By exploring at different growth parameters, we have determined the growth mechanisms. We find that a high gallium rate is important for achieving high aspect ratio structures and (110)-type of facets. The functionality of the membranes is further demonstrated by showing bright luminescence of the membranes and the associated quantum heterostructures. Our analysis further proves the potential of this new kind of nanostructure for future optoelectronic studies.

Acknowledgements

GT, HP, FM and AFiM acknowledge SNF funding through the NCCR QSIT, its director's reserve and project nr 143908 and 134506 (DACH program), as well as CIME and CMI for access to the electron microscopes. Some of the research leading to these results has received funding from the European Union Seventh Framework Program under Grant Agreement 312483 - ESTEEM2 (Integrated Infrastructure Initiative – I3). JA and MdlM acknowledge the funding from the Spanish MINECO MAT2014-51480-ERC (e-ATOM) and Severo Ochoa Excellence Program and Generalitat de Catalunya 2014SGR1638. MdlM thanks the CSIC Jae-Predoc program. The STEM and FIB sample preparation works have been conducted partially in the "Laboratorio de Microscopias Avanzadas" at "Instituto de Nanociencia de Aragon - Universidad de Zaragoza". Authors acknowledge the LMA-INA for offering access to their instruments and expertise. Authors also acknowledge ICN2 for the use of their microscopy facilities.

Notes and references

‡ Footnotes relating to the main text should appear here. These might include comments relevant to but not central to the matter under discussion, limited experimental and spectral data, and crystallographic data.

References

1 J. Wallentin, N. Anttu, D. Asoli, M. Huffman, I. Åberg, M. H. Magnusson, G. Siefer, P. Fuss-Kailuweit, F. Dimroth, B. Witzigmann, H. Q. Xu, L. Samuelson, K. Deppert and M. T. Borgström, *Science*, 2013, **339**, 1057–1060.
2 V. Mourik, K. Zuo, S. M. Frolov, S. R. Plissard, E. P. a. M. Bakkers and L. P. Kouwenhoven, *Science*, 2012, **336**, 1003–1007.
3 P. Krogstrup, H. I. Jørgensen, M. Heiss, O. Demichel, J. V. Holm, M. Aagesen, J. Nygard and A. Fontcuberta i Morral, *Nat. Photonics*, 2013, **7**, 306–310.
4 F. Patolsky and C. M. Lieber, *Mater. Today*, 2005, **8**, 20–28.
5 S. R. Plissard, I. van Weperen, D. Car, M. A. Verheijen, G. W. G. Immink, J. Kammhuber, L. J. Cornelissen, D. B. Szombati, A. Geresdi, S. M. Frolov, L. P. Kouwenhoven and E. P. A. M. Bakkers, *Nat. Nanotechnol.*, 2013, **8**, 859–864.
6 H. A. Atwater and A. Polman, *Nat. Mater.*, 2010, **9**, 205–213.
7 P. Krogstrup, N. L. B. Ziino, W. Chang, S. M. Albrecht, M. H. Madsen, E. Johnson, J. Nygard, C. M. Marcus and T. S. Jespersen, *Nat. Mater.*, 2015, **14**, 400–406.
8 A. Fontcuberta i Morral, D. Spirkoska, J. Arbiol, M. Heigoldt, J. R. Morante and G. Abstreiter, *Small*, 2008, **4**, 899–903.
9 M. Heiss, Y. Fontana, A. Gustafsson, G. Wüst, C. Magen, D. D. O'Regan, J. W. Luo, B. Ketterer, S. Conesa-Boj, A. V. Kuhlmann, J. Houel, E. Russo-Averchi, J. R. Morante, M. Cantoni, N. Marzari, J. Arbiol, A. Zunger, R. J. Warburton and A. Fontcuberta i Morral, *Nat. Mater.*, 2013, **12**, 439–444.
10 J. Arbiol, C. Magen, P. Becker, G. Jacopin, A. Chernikov, S. Schäfer, F. Furtmayr, M. Tchernycheva, L. Rigutti, J. Teubert, S. Chatterjee, J. R. Morante and M. Eickhoff, *Nanoscale*, 2012, **4**, 7517–7524.
11 K. A. Dick, K. Deppert, M. W. Larsson, T. Mårtensson, W. Seifert, L. R. Wallenberg and L. Samuelson, *Nat. Mater.*, 2004, **3**, 380–384.
12 M. I. B. Utama, M. de la Mata, C. Magen, J. Arbiol and Q. Xiong, *Adv. Funct. Mater.*, 2013, **23**, 1636–1646.
13 F. Schuster, M. Hetzl, S. Weiszer, J. A. Garrido, M. de la Mata, C. Magen, J. Arbiol and M. Stutzmann, *Nano Lett.*, 2015, **15**, 1773–1779.
14 Y. Cui, U. Banin, M. T. Björk and A. P. Alivisatos, *Nano Lett.*, 2005, **5**, 1519–1523.
15 R. R. Zamani, M. Ibáñez, M. Luysberg, N. García-Castelló, L. Houben, J. D. Prades, V. Grillo, R. E. Dunin-Borkowski, J. R. Morante, A. Cabot and J. Arbiol, *ACS Nano*, 2014, **8**, 2290–2301.
16 S. Conesa-Boj, E. Russo-Averchi, A. Dalmau-Mallorqui, J. Trevino, E. F. Pecora, C. Forestiere, A. Handin, M. Ek, L. Zweifel, L. R. Wallenberg, D. Rüffer, M. Heiss, D. Troadec, L. Dal Negro, P. Caroff and A. Fontcuberta i Morral, *ACS Nano*, 2012, **6**, 10982–10991.
17 M. Aagesen, E. Johnson, C. B. Sørensen, S. O. Mariager, R. Feidenhans'l, E. Spiecker, J. Nygård and P. E. Lindelof, *Nat. Nanotechnol.*, 2007, **2**, 761–764.
18 W. Seifert, M. Borgström, K. Deppert, K. A. Dick, J. Johansson, M. W. Larsson, T. Mårtensson, N. Sköld, C. Patrik T. Svensson, B. A. Wacaser, L. Reine Wallenberg and L. Samuelson, *J. Cryst. Growth*, 2004, **272**, 211–220.
19 T.-W. Yeh, Y.-T. Lin, B. Ahn, L. S. Stewart, P. D. Dapkus and S. R. Nutt, *Appl. Phys. Lett.*, 2012, **100**, 033119.
20 A. K. Rishinaramangalam, S. M. U. Masabih, M. N. Fairchild, J. B. Wright, D. M. Shima, G. Balakrishnan, I. Brener, S. R. J. Brueck and D. F. Feezell, *J. Electron. Mater.*, 2014, **44**, 1255–1262.
21 E. F. Pecora, G. F. Walsh, C. Forestiere, A. Handin, E. Russo-Averchi, A. Dalmau-Mallorqui, I. Canales-Mundet, A. F. i Morral and L. D. Negro, *Nanoscale*, 2013, **5**, 10163–10170.
22 K. A. Dick, C. Thelander, L. Samuelson and P. Caroff, *Nano Lett.*, 2010, **10**, 3494–3499.
23 P. Caroff, K. A. Dick, J. Johansson, M. E. Messing, K. Deppert and L. Samuelson, *Nat. Nanotechnol.*, 2009, **4**, 50–55.
24 P. Caroff, J. Bolinsson and J. Johansson, *IEEE J. Sel. Top. Quantum Electron.*, July-Aug., **17**, 829–846.
25 Q. Gao, D. Saxena, F. Wang, L. Fu, S. Mokkapati, Y. Guo, L. Li, J. Wong-Leung, P. Caroff, H. H. Tan and C. Jagadish, *Nano Lett.*, 2014, **14**, 5206–5211.
26 D. Jacobsson, S. Lehmann and K. A. Dick, *Nanoscale*, 2014, **6**, 8257–8264.

Nanoscale Accepted Manuscript

27 R. E. Algra, M. A. Verheijen, M. T. Borgström, L.-F. Feiner, G. Immink, W. J. P. van Enckevort, E. Vlieg and E. P. A. M. Bakkers, *Nature*, 2008, **456**, 369–372.
28 E. Gil, V. G. Dubrovskii, G. Avit, Y. André, C. Leroux, K. Lekhal, J. Grecenkov, A. Trassoudaine, D. Castelluci, G. Monier, R. M. Ramdani, C. Robert-Goumet, L. Bideux, J. C. Harmand and F. Glas, *Nano Lett.*, 2014, **14**, 3938–3944.
29 M. de la Mata, C. Magen, J. Gazquez, M. I. B. Utama, M. Heiss, S. Lopatin, F. Furtmayr, C. J. Fernández-Rojas, B. Peng, J. R. Morante, R. Rurali, M. Eickhoff, A. Fontcuberta i Morral, Q. Xiong and J. Arbiol, *Nano Lett.*, 2012, **12**, 2579–2586.
30 J. Arbiol, S. Estradé, J. D. Prades, A. Cirera, F. Furtmayr, C. Stark, A. Laufer, M. Stutzmann, M. Eickhoff, M. H. Gass, A. L. Bleloch, F. Peiró and J. R. Morante, *Nanotechnology*, 2009, **20**, 145704.
31 J. Bao, D. C. Bell, F. Capasso, J. B. Wagner, T. Mårtensson, J. Trägårdh and L. Samuelson, *Nano Lett.*, 2008, **8**, 836–841.
32 M. D. Stiles and D. R. Hamann, *Phys. Rev. B*, 1990, **41**, 5280–5282.
33 K. Ikejiri, T. Sato, H. Yoshida, K. Hiruma, J. Motohisa, S. Hara and T. Fukui, *Nanotechnology*, 2008, **19**, 265604.
34 H. Yoshida, K. Ikejiri, T. Sato, S. Hara, K. Hiruma, J. Motohisa and T. Fukui, *J. Cryst. Growth*, 2009, **312**, 52–57.
35 J. N. Shapiro, A. Lin, C. Ratsch and D. L. Huffaker, *Nanotechnology*, 2013, **24**, 475601.
36 C.-Y. Chi, C.-C. Chang, S. Hu, T.-W. Yeh, S. B. Cronin and P. D. Dapkus, *Nano Lett.*, 2013, **13**, 2506–2515.
37 S. Arab, C.-Y. Chi, T. Shi, Y. Wang, D. P. Dapkus, H. E. Jackson, L. M. Smith and S. B. Cronin, *ACS Nano*, 2015, **9**, 1336–1340.
38 C.-C. Chang, C.-Y. Chi, C.-C. Chen, N. Huang, S. Arab, J. Qiu, M. L. Povinelli, P. D. Dapkus and S. B. Cronin, *Nano Res.*, 2014, **7**, 163–170.
39 C. A. Schneider, W. S. Rasband and K. W. Eliceiri, *Nat. Methods*, 2012, **9**, 671–675.
40 S. Bernal, F. J. Botana, J. J. Calvino, C. López-Cartes, J. A. Pérez-Omil and J. M. Rodríguez-Izquierdo, *Ultramicroscopy*, 1998, **72**, 135–164.
41 J. Arbiol, A. Cirera, F. Peiró, A. Cornet, J. R. Morante, J. J. Delgado and J. J. Calvino, *Appl. Phys. Lett.*, 2002, **80**, 329–331.
42 M. Heiß, E. Riedlberger, D. Spirkoska, M. Bichler, G. Abstreiter and A. F. i Morral, *J. Cryst. Growth*, 2008, **310**, 1049–1056.
43 C. Colombo, D. Spirkoska, M. Frimmer, G. Abstreiter and A. F. I. Morral, *Phys. Rev. B*, 2008, **77**, 155326.
44 K. Tomioka, P. Mohan, J. Noborisaka, S. Hara, J. Motohisa and T. Fukui, *J. Cryst. Growth*, 2007, **298**, 644–647.
45 M. T. Borgström, G. Immink, B. Ketelaars, R. Algra and E. P. A. M. Bakkers, *Nat. Nanotechnol.*, 2007, **2**, 541–544.
46 S. J. Gibson and R. R. LaPierre, *Nanotechnology*, 2014, **25**, 415304.
47 D. Rudolph, L. Schweickert, S. Morkötter, B. Loitsch, S. Hertenberger, J. Becker, M. Bichler, G. Abstreiter, J. J. Finley and G. Koblmüller, *Appl. Phys. Lett.*, 2014, **105**, 033111.
48 M. R. Ramdani, J. C. Harmand, F. Glas, G. Patriarche and L. Travers, *Cryst. Growth Des.*, 2013, **13**, 91–96.
49 T. Takebe, M. Fujii, T. Yamamoto, K. Fujita and T. Watanabe, *J. Appl. Phys.*, 1997, **81**, 7273–7281.
50 S.-C. Lee, K. J. Malloy and S. R. J. Brueck, *J. Appl. Phys.*, 2001, **90**, 4163–4168.
51 N. Sköld, J. B. Wagner, G. Karlsson, T. Hernán, W. Seifert, M.-E. Pistol and L. Samuelson, *Nano Lett.*, 2006, **6**, 2743–2747.
52 D. A. Woolf, Z. Sobiesierski, D. I. Westwood and R. H. Williams, *J. Appl. Phys.*, 1992, **71**, 4908–4915.

Nanoscale Accepted Manuscript

This journal is © The Royal Society of Chemistry 20xx

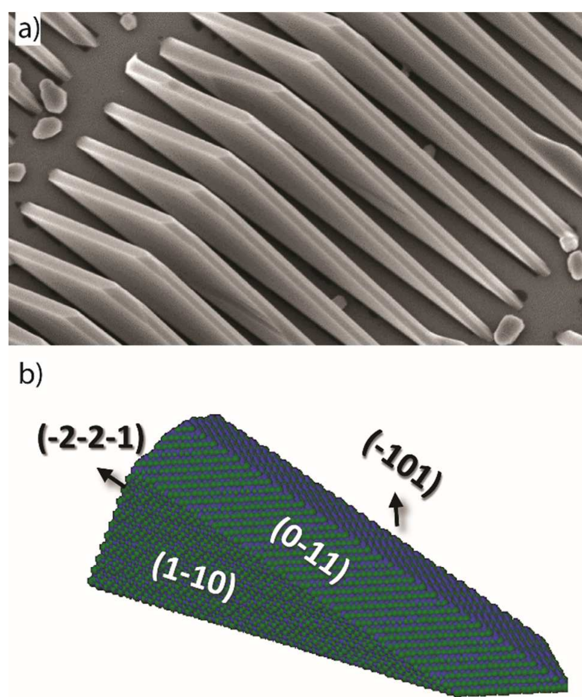

Figure 1:

a) SEM image of a GaAs nanomembrane array
b) 3D model of the grown structures

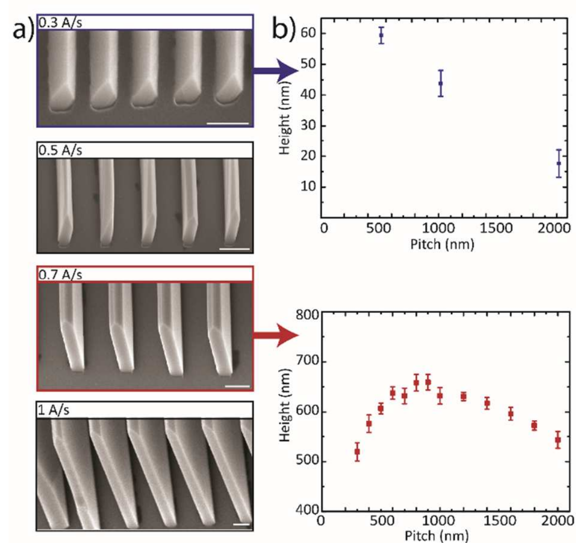

Figure 2:

a) Close-up SEM images of GaAs nanomembranes grown with different Gallium rates. (Scale bar is 200 nm)
b) Pitch dependency of two samples grown with 0.3A/s and 0.7A/s Gallium rates

Nanoscale Accepted Manuscript

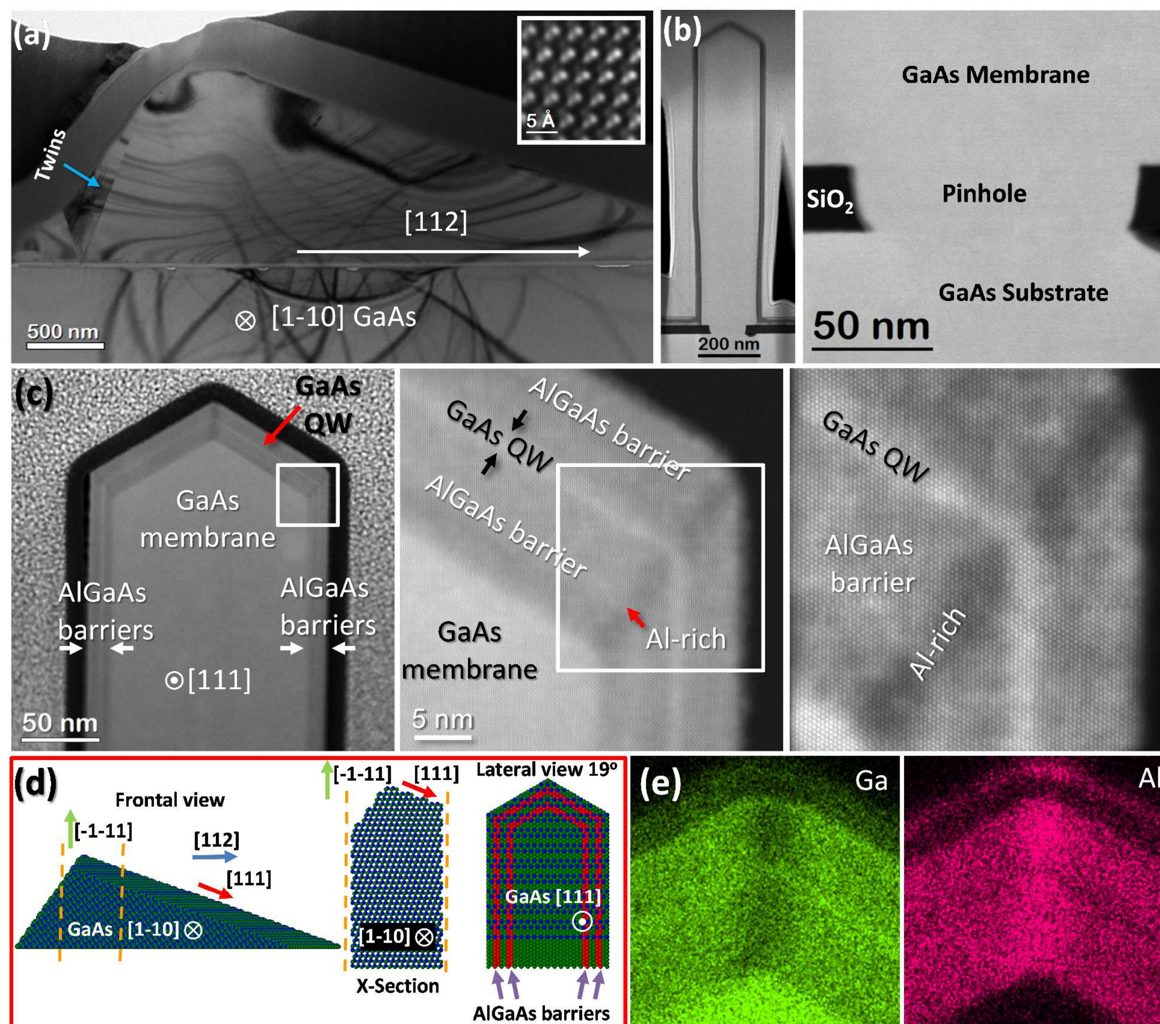

Figure 3:

a) TEM image of the membrane cross-section showing pure ZB phase. Notice the presence of a small region (pointed with a blue arrow) showing twins. The upper right inset corresponds to an atomic resolution HAADF STEM image of the pure ZB structure of the membranes showing a clear B-polarity (As on top).
b) HAADF-STEM general view of the membrane cross-section (left). On the right, we show a close up of the formation of the opening in the oxide.
c) (left) HAADF-STEM image of the membrane cross-section obtained at 19° (along the [111] axis) in order to visualize the formation of QWs on the front and back <110> flat surfaces as well as on the top <110> surfaces. (Middle) Atomic resolution HAADF STEM magnified image of the region squared in (left). (right) Atomic resolution HAADF STEM close up image of the region squared in (middle). Notice the perfect formation of the QWs and the AlGaAs barriers and the Al-rich stripe on one of the <112> corners.
d) Indexed atomic 3D model of an entire nanomembrane and the corresponding model for the FIB cut in lateral and front views. e) Al and Ga EDX elemental maps obtained on the tip of the nanomembrane cross-section shown in c).

Nanoscale Accepted Manuscript

This journal is © The Royal Society of Chemistry 20xx

Please do not adjust margins

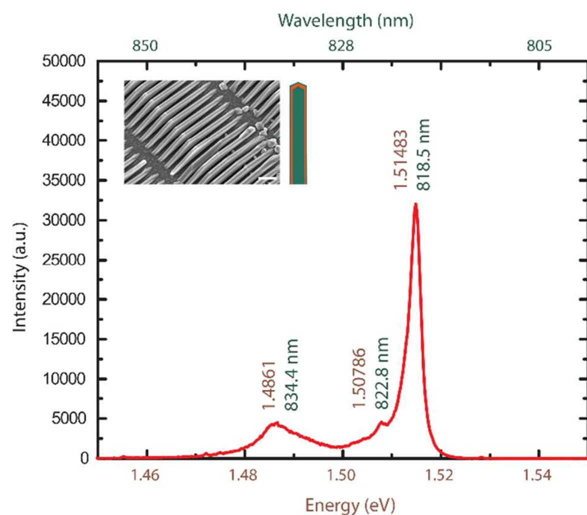

Figure 4:
PL spectrum of GaAs/AlGaAs core/shell nanomembrane based heterostructure (SEM image of the array and cross-section of the heterostructure are shown in inset)

a)

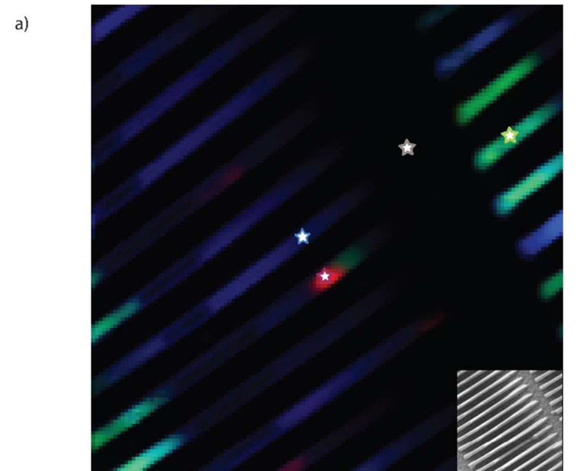

b)

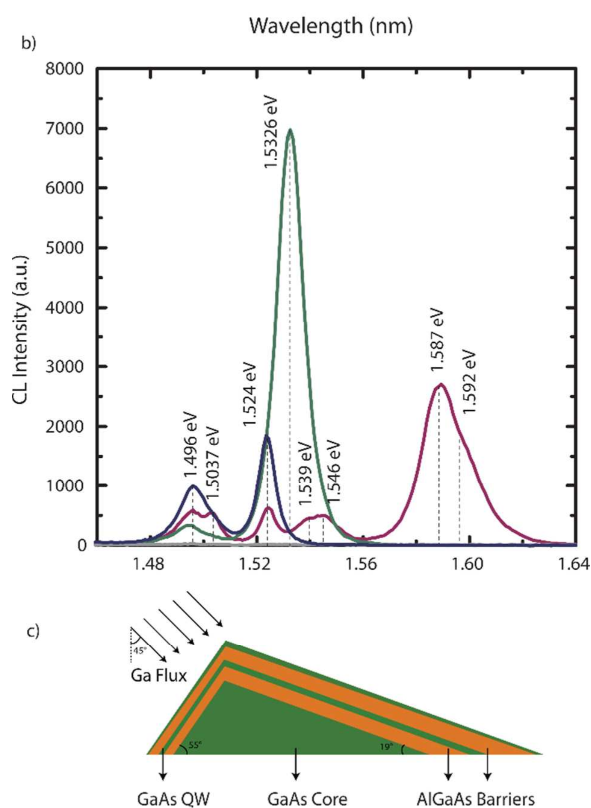

Figure 5:

a) CL mapping of GaAs/AlGaAs heterostructure with GaAs QWs
b) Point spectra collected from the same colour marked regions
c) Axial cross-section of the QW structure showing incoming fluxes

Nanoscale Accepted Manuscript

Please do not adjust margins